Journal of The Electrochemical Society, **148** (7) A762-A767 (2001)
0013-4651/2001/148(7)/A762/6/$7.00 © The Electrochemical Society, Inc.

Comparison of the Electrochemical Impedance Spectroscopy Characteristics of Insertion Electrode Materials Used in Secondary Metal Hydride and Lithium-Ion Electrodes

Chunsheng Wang,[a,*,z] A. John Appleby,[a,*] and Frank E. Little[b]

[a]*Center for Electrochemical Systems and Hydrogen Research,* [b]*Center for Space Power, Texas Engineering Experiment Station, Texas A&M University, College Station, Texas 77843, USA*

$LaNi_{4.4}Sn_{0.25}$ and graphite powder disk electrodes sandwiched between two nickel screens were used as working electrodes in 6.0 M KOH and in 1.0 M $LiPF_6$ in propylene carbonate-ethylene carbonate-dimethyl carbonate (1:1:3) solution, respectively. Different electrochemical impedance spectroscopy protocols were used for analysis of the kinetics of insertion and extraction of hydrogen and lithium into these materials and accompanying changes in intrinsic electrode resistance. The imaginary *vs.* real impedance plots for both electrodes show a high frequency depressed semicircle, a midfrequency charge transfer semicircle, then an inclined line for reactant diffusion in the host structure. In both cases, the first semicircle was not a result of particle-to-current collector and particle-to-particle contact impedance, although part of the contact impedance is shown to be in series with the kinetic impedance.
 [DOI: 10.1149/1.1377285]

Manuscript submitted July 28, 2000; revised manuscript received February 26, 2001. Available electronically June 8, 2001.

Many ambient temperature secondary cells, including nickel-metal hydride (Ni-MH) and lithium ion (Li ion) types, contain insertion materials. The reason for their broad application is because electrochemical insertion reactions are intrinsically simple and rather reversible.[1] AB_5 phase intermetallic compounds and graphite are the most common host materials in commercial Ni-MH and Li-ion anodes because of their high capacities (coincidentally, 372 mAh/g for both $LaNi_5H_6$ and LiC_6), excellent cycling capability with low volume expansion during H or Li insertion/extraction, and low cost.

Both host materials carry surface films under insertion conditions, an oxide film on AB_5 compounds, and the solid electrolyte interphase (SEI) film resulting from organic electrolyte decomposition on graphite. Electrochemical hydrogen insertion into AB_5 compounds in aqueous media is similar to that of Li into graphite under aprotic conditions when the AB_5 particle oxide film thickness is greater than the electron tunneling length. In both cases, the reactant species H_2O and Li^+ move through the electrolyte, then through a film of low electronic conductivity, followed by charge transfer to and insertion. If the hydrated oxide film on hydride particles is thinner than the electron tunneling length, charge transfer will occur on the oxide film surface, with movement of hydrogen from an adsorption site at the film surface to an absorption site below the surface.[2]

Extensive kinetic measurements for both metal-hydride[3-9] and Li-graphite[10-14] electrodes have been conducted because these determine battery power densities. Electrochemical impedance spectroscopy (EIS) is a more powerful technique than, *e.g.*, potential intermittent titration (PITT), galvanostatic intermittent titration (GITT), Tafel polarization, or linear micropolarization because it can give the individual impedances for each reaction step if these have separable time constants. Typical imaginary *vs.* real impedance plots for metal hydride and Li-graphite electrodes show two depressed semicircles in the high to midfrequency region and an inclined line at low frequencies. It is generally believed that the second (midfrequency) semicircle is related to charge transfer, while the sloping line is attributed to reactant diffusion in the host materials. However, there is disagreement on the interpretation of the first (high frequency) semicircle. Some authors attribute it to the contact impedance between the current collector and the host particles in both hydride[4,8,9] and Li-graphite electrodes.[12] Others consider it to be associated with the transition of hydrogen between absorption sites in hydride electrodes,[5-7] and with Li^+ movement through the SEI film for Li-graphite electrodes.[10,11,13,14]

Experimental

Disk electrodes of 2 cm^2 geometric area containing *ca.* 50 mg of JM 287 graphite powder (15 μm particle size, Brunauer, Emmett, Teller area 13.5 $m^2\,g^{-1}$, Johnson Matthey, Inc.) with 8 wt % polyvinylidene fluoride binder in ethyl-2-pyrrolidinone and 75 mg $LaNi_{4.4}Sn_{0.25}$ powder (<45 μm) with 50 mg of Teflonized Vulcan XC-72R conducting furnace black (Cabot Corporation) and 25 mg of poly(tetrafluorethylene) (PTFE) powder were sandwiched between two nickel screens. They were used as working electrodes in 1.0 M lithium hexafluorophosphate ($LiPF_6$) in a 1:1:3 by volume mixture of ethylene carbonate (EC)-propylene carbonate (PC)-dimethylcarbonate (DMC) (high purity lithium battery grade, Mitsubishi Chemical Company) and in 6 M KOH solution, respectively. The configuration of a typical electrode has been given in Fig. 1. The equipment and preparative and electrochemical procedures used have been described.[15-19] Charge discharge of the graphite electrode was between +0.0 and +1.5 V *vs.* Li at 5 mA/g, while $LaNi_{4.4}Sn_{0.25}$ was charged at 100 mA/g for 3.5 h and discharged at 50 mA/g to −0.6 V *vs.* Hg/HgO at room temperature. The origin of the first (high frequency) semicircle was investigated using different EIS

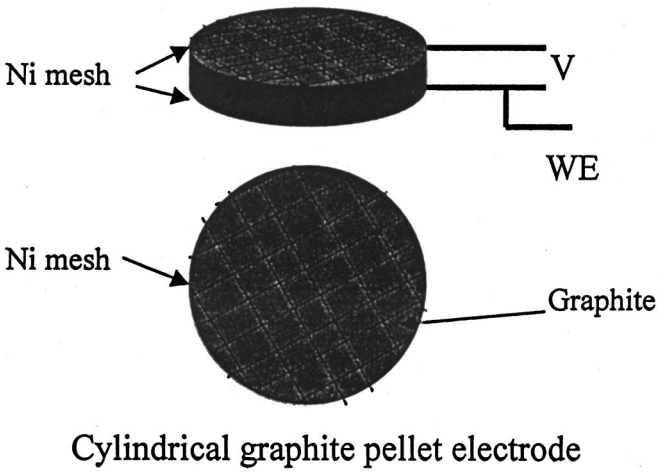

Figure 1. Schematic diagram of graphite electrode configuration.

* Electrochemical Society Active Member.
z E-mail: cswang@tamu.edu

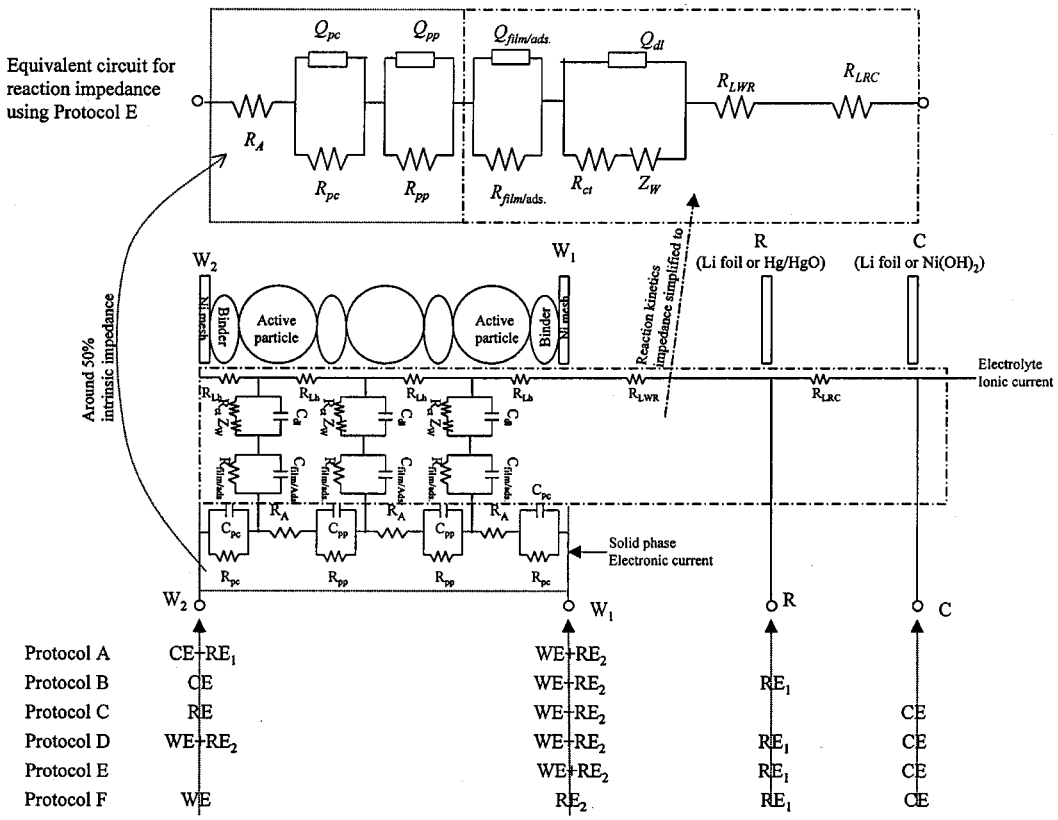

Figure 2. Schematic diagram of cell with porous ion insertion anode and special Solatron electrochemical interface terminal-to-electrode connections. The transmission line equivalent circuit and simplified equivalent circuit for ion insertion/extraction into active electrode is also shown. R_A, R_{Lh}, R_{WR}, and R_{RC}: Electronic resistance of active particle, ion resistance of electrolytes in the pores, reference electrode to working electrode ionic resistance, and reference electrode to counter electrode ionic resistance. R_{pc}, R_{pp}, $R_{film/ads}$ and R_{ct}: Active particles-to-current collector, particles-to-particles, film (SEI film for graphite anode and oxide film or H adsorption/absorption for hydride electrode), and charge-transfer resistances. C_{pc} and C_{pp}: Particles-to-current collector and particles-to-particles contact capacitances. $Q_{film/ads.}$ and Q_Z: Constant phase elements for the film (or H ads/abs) and for the double layer, respectively. Z_W: Finite Warburg element for lithium or hydrogen diffusion in graphite.

connection protocols, each over the frequency range 65 kHz to 1.0 mHz at a potentiostatic signal amplitude of 5 mV at different state of discharge after 6 charge/discharge cycles for the $LaNi_{4.4}Sn_{0.25}$ electrode and after 14 cycles for the graphite electrode. This was to allow a stable SEI film to form on the graphite electrode, and to fully activate the $LaNi_{4.4}Sn_{0.25}$ alloy. Reaction kinetic parameters were also obtained from EIS measurements.

Two types of impedance, namely, ''transmissive'' impedance, and electrochemical reaction kinetic impedance, were measured for porous electrode. For the transmissive impedance measurements, EIS scans were taken in three ways using three different methods of connecting the interface terminals: between the two sides of the working electrode, connecting the RE_2 and WE terminals of the Solatron interface together to one side and RE_1 and CE to the other (protocol A); with RE_2 and WE connected to one side and CE to the other, with a reference electrode connected to RE_1 (protocol B); and with RE_2 and WE connected to one side and RE_1 to the other, with a counter electrode connected to CE (protocol C). The three electrochemical kinetic EIS measurements were taken. First, terminals RE_2 plus WE were connected to both sides of the working electrode (protocol D); then terminals RE_2 plus WE were connected to one side only (protocol E); and finally terminal RE_2 was connected to one side and terminal WE to the other (protocol F). A schematic diagram of the cell and the different interface terminal-to-electrode connections, including the geometrical arrangement of the counter and reference electrodes for each protocol, is shown in Fig. 2.

After the six EIS protocols were completed, the 0.135 mm thick $LaNi_{4.4}Sn_{0.25}$ electrode was subjected to adjustable compression using a stainless steel screw between two 3.5 mm thick PTFE holders containing small holes to allow entry of electrolyte. The EIS protocols were then repeated on the compressed electrode to investigate the influence of contact impedance on kinetic impedance. All impedances measured were normalized to the weight of the active material in the electrode.

Results and Discussion

Physical meaning of the six EIS protocols for porous ion insertion electrodes.—The active particles in the macroscopically homogeneous electrodes are connected to other particles and to the current collectors by a binder, and are interconnected to the electrolyte filling the pores between them. The ionic currents result from motion of Li^+ from the cathode to the anode, then through the SEI film, followed by charge transfer and Li insertion, and motion of H_2O^+ from the cathode to the anode, charge transfer to OH^- and H, insertion through adsorb-absorb transition, followed by movement of OH^- from anode to cathode. The electronic current passes from particle to particle and then to the current collectors, and the equal and opposite ionic current flows between the particles to the bulk electrolyte. Thus, the intrinsic impedance is in series with the reaction impedance in each transmission line unit. The ionic impedance is considered to be part of the reaction impedance. The transmission line equivalent circuit of the porous insertion electrode[20] shown in Fig. 2 is modified to take into account the particle-to-particle and particle-to-current collector contact impedances.[15-19] The distance traveled by the electrochemical current in the electrode depends on the distance of particles from the current collector. The average

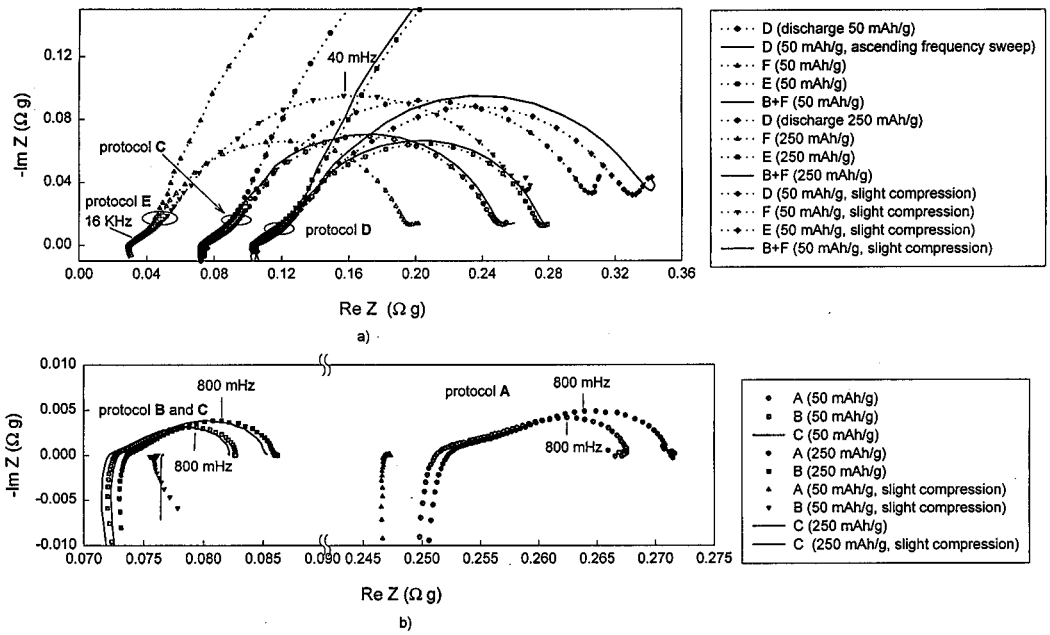

Figure 3. Electrochemical impedance spectroscopy of the $LaNi_{4.4}Sn_{0.25}$ electrode at the 20 and 100% discharge states using different Solatron electrochemical interface terminal-to-electrode connections in Fig. 1. (a) Kinetics of electrochemical hydrogen insertion-extraction, (b) intrinsic (or transmission) impedance of $LaNi_{4.4}Sn_{0.25}$ electrode. Slight compression of the $LaNi_{4.4}Sn_{0.25}$ electrode was conducted by using two PTFE holders on each side of the electrode, each containing small holes to allow entry of electrolyte. Before measurement the electrode was cycled six times, and allowed to rest for 1 h.

intrinsic impedance in series with the reaction kinetic EIS is about half of the overall intrinsic impedance for active particles homogeneously interconnected at a macroscopic level. The average reaction impedance of electrode can be obtained from the summation of individual parallel impedances if the influence of intrinsic impedance on reaction impedance can be neglected. Because of the spatial distribution of the active particles, the capacitances are replaced by constant phase elements (CPEs) denoted as *Q* (see Fig. 2) for the averaged reaction impedance using protocol E.

It is clear from Fig. 2 that the protocol E EIS reflects the electrochemical reaction impedance of the porous electrode, with approximately 50% of the intrinsic impedance in series with it. The EIS using protocol E becomes that for protocol D if the Solatron terminal WE + RE_2 is connected to both side of the electrode, and protocol E becomes protocol F if terminal RE_2 is moved from the W_1 to W_2 side of the electrode in protocol E. The active particle-to-current collector distance in protocol E is effectively double that in protocol D, whereas the particle-to-current collector area is halved, so the intrinsic impedance in series with the reaction kinetic impedance in protocol E should be twice that for protocol D. Finally, protocol F automatically eliminates the in-series intrinsic impedance.

When measured using protocol A, the reaction impedance is in parallel with intrinsic impedance in each transmission line unit (the transmissive impedance, including the active particle electronic impedances, and the particle-to-particle and particle-to-current collector contact impedances). The intrinsic impedance is usually much smaller than the reaction impedance. The influence of reaction impedance on transmissive impedance is therefore small, so protocol A effectively determines the intrinsic impedance. Then the particle electronic resistances, the particle-to-particle resistances, and the particle-to- current collector contact resistances may be obtained, respectively, from protocol A EIS measurements by the intersections of the high frequency line and of the first and second semicircles with the real axis.[15-19] However, if the intrinsic impedance is high because of exfoliation of graphite or alloy pulverization, the protocol A measurement will not give the intrinsic impedance. It may even represent the reaction impedance with one portion of the electrode acting as an anode and another as a cathode.[18]

To measure the intrinsic impedance in series with the reaction impedance using protocol E, the reaction impedance must be eliminated from the protocol E EIS. One way to do this is to use an electronic transelectrode current to replace the ionic current in the electrolyte by moving terminal CE from the counter electrode to the W_2 side of electrode, as in protocol B. As with protocol A, the series reaction impedance also partly involved in the protocol B EIS, but if the intrinsic impedance is much smaller than the reaction impedance, protocol B can still give the intrinsic impedance which is in series with the reaction impedance obtained using protocol E.

Another way to eliminate the reaction impedance from the protocol E EIS is to use the reference voltage signal from both sides of the electrode while the ionic current passes through the electrode, *i.e.*, by moving terminal RE_1 from the reference electrode to W_2 side of electrode in protocol E to give protocol D, whose EIS also reflects the intrinsic impedance which is in series with the reaction impedance obtained using protocol E.

The six EIS protocols have the following physical meanings and characteristics:[17]

1. When the intrinsic impedance is much smaller than the reaction impedance, the intrinsic impedance of porous electrode can be obtained by using protocol A, and the intrinsic impedance involved in the reaction impedance can be measured using protocols B and C. The protocol B impedance should be equal to that for protocol C, but half of that for protocol A.

2. The intrinsic impedance for protocol F is zero, whereas that for protocol D should be half of that for protocol E. Therefore the EIS spectra for protocol D should lie between those for protocol E and F, since the intrinsic impedance is then in series with the reaction EIS (Fig. 2).

3. The impedance using protocol E should be equal to the sum of the impedances using protocol F and B (or C).

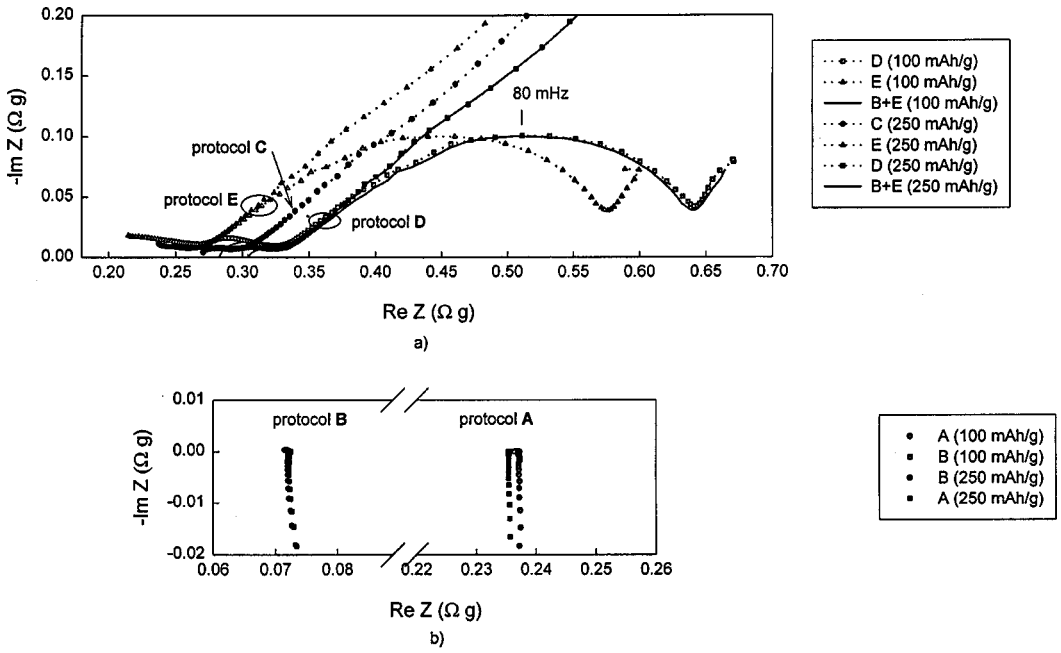

Figure 4. Electrochemical impedance spectroscopy for the heavily compressed $LaNi_{4.4}Sn_{0.25}$ electrode in the 40 and 100% discharge states using different Solatron electrochemical interface terminal-to-electrode connections in Fig. 1. (a) Kinetics of electrochemical hydrogen insertion-extraction, (b) intrinsic (or transmission) impedance of the compressed $LaNi_{4.4}Sn_{0.25}$ electrode. High compression was achieved by decreasing the distance between the two PTFE holders. Before measurement, the electrode was cycled six times uncompressed, then cycled two times under pressure.

EIS of $LaNi_{4.4}Sn_{0.25}$ porous metal-hydride electrode.—The discharge capacity of the $LaNi_{4.4}Sn_{0.25}$ electrode increased with increasing charge/discharge cycling and reached 252 mAh/g at 6 cycles as alloy activation progressed. It then began to gradually decrease on further cycling. The cycling behavior of $LaNi_{4.4}Sn_{0.25}$ was similar to that of the $LaNi_{4.75}Sn_{0.25}$ electrode reported by Ratnakumar.[3] The lower capacity of $LaNi_{4.4}Sn_{0.25}$ compared to that of $LaNi_{4.75}Sn_{0.25}$ (300 mAh/g) may be attributed to the different nickel content. After the electrode reached its maximum capacity at 6 cycles, the six EIS protocols were conducted on the $LaNi_{4.4}Sn_{0.25}$ electrode in the 20% and 100% discharge states. Previous work has shown that metal hydride electrodes are stable linear systems, which show little change in properties during the periods required for EIS studies.[4] This has been confirmed by Kramers-Kronig transforms,[4] by the nearly identical impedance spectra using descending and ascending frequencies between 65 kHz to 0.001 Hz, and by using different excitation voltages (3 to 8 mV).[19]

Figures 3 and 4 show the results of the three protocols used for $LaNi_{4.4}Sn_{0.25}$ kinetic impedance measurements, and of the three for intrinsic impedance after 6 cycles under no compression, and in slightly and highly compressed states. The three protocols (D, E, and F) for reaction kinetic EIS determinations (Fig. 3a and 4a) show typical hydride EIS characteristics, *i.e.*, two depressed semicircles in high frequency regions and an inclined line at low frequencies. The second semicircle, corresponding to the charge transfer reaction, was overlapped by the H diffusion line when the electrode was fully discharged. Slight compression of the electrode increased the charge transfer resistance slightly, but had no influence on the size of the first semicircle. However, the first semicircle became larger if the compression was further increased (Fig. 4a). The increase in size of the second semicircle (corresponding to the charge transfer reaction) on compression may attributed to the carbon black covering a larger area of the alloy surface, giving a reduced electrochemical reaction area. Two depressed semicircles were observed in the three protocols (A, B, and C) for intrinsic impedance measurement (Fig. 3b). These two semicircles were mainly characteristic of the particle-to-particle and particle-to-current collector contact impedance,[15-19] and did not involve the reaction impedance. This is because the characteristic frequency at the imaginary semicircle maximum for protocols A, B, and C is much higher than that for protocols D, E, and F, and an increase in compression increased charge transfer impedance (Fig. 3a) but decreased the semicircle dimensions in the protocol A impedance. Compression of the electrode improved the contact conductivity, as is shown in Fig. 3b. The second semicircle in the low frequency region in the fully discharged state (*i.e.*, after discharge of 250 mAh/g) is larger than that for the 20% discharged state (Fig. 3b). This may be explained by the high particle-to-particle contact resistance resulting from the volume shrinkage after hydrogen desorption from the electrode. The resistance determined from the intersection of the high-frequency line with the real axis in Fig. 3b and 4b was attributed to the total electronic resistance of the metal-hydride particles.[16] Compression had little influence on the total electronic resistance of the $LaNi_{4.4}Sn_{0.25}$ particles although it decreased the contact resistances. The inductive reactances in the high frequency range in Fig. 3 and 4b are not associated with the electrode, but are artifacts resulting from the Solartron equipment used.[16] Although contact resistances exist between the current collector and the metal hydride powder, it is difficult to attribute the high frequency semicircle in Fig. 3a and 4a to a contact resistance for the following reasons: (*i*) the total contact resistance for the zero compression case in Fig. 3b is much higher than the resistance shown in the high frequency range in Fig. 3a; (*ii*) the characteristic frequency (800 mHz) for the contact impedance in Fig. 3b is much smaller than the 16 kHz value in the high frequency range in Fig. 3a; (*iii*) compressing the electrode reduced the intrinsic electrode resistance (Fig. 3b and 4b), but increased the resistance in the high frequency range (compare Fig. 3a and 4a); (*iv*) extraction of hydrogen from $LaNi_{4.4}Sn_{0.25}H_x$ electrode reduces the alloy volume, increasing the contact resistance (Fig. 3b), but it has no influence on the size of the first kinetic impedance semicircle (Fig. 3a); and (*v*) if the first high frequency reaction kinetic impedance semicircle corresponds to contact resistance, the diameter of first semicircle in the protocol E should be twice that of the protocol D because the metal-hydride particle-current collector area is thereby doubled. The first semi-

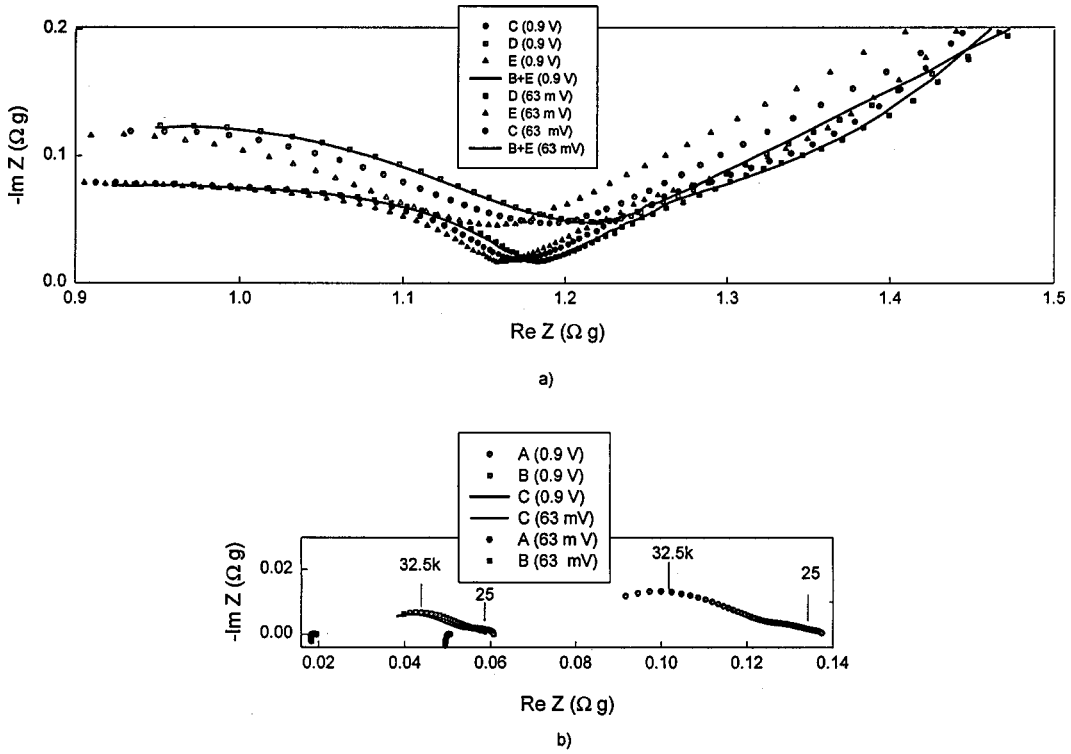

Figure 5. EIS of JM 287 graphite at 0.9 and 0.063 V using different Solatron electrochemical interface terminal-to-electrode connections shown in Fig. 1. (a) Kinetics of electrochemical lithium insertion-extraction, (b) intrinsic (or transmission) impedance of JM 287 graphite. Before measurement the electrode was cycled 17 times, then allowed to rest for 2 h.

circle should then not be present in protocol F measurements, because its connections automatically eliminate the intrinsic resistance of the graphite electrode. However the first depressed semicircle is present in the protocol F EIS (Fig. 3a and 4a), and it has similar sizes for both the D and E protocols. The first semicircle for D lies mid-way between those for F and E, but is not half of the size of that for D. Therefore, the results in Fig. 3 and 4 results strongly suggest that the first kinetic impedance semicircle should not be directly attributed to the contact resistance.

As expected, results of the $LaNi_{4.4}Sn_{0.25}$ electrode in Fig. 3 and 4 also show that

1. The protocol D impedance lies midway between those obtained using protocol E and F.
2. The impedance measured using protocol E is almost equal to the sum of the impedances using protocols F and B or F and C.
3. The protocol B impedance is almost equal to that obtained using protocol C, and is 30-50% of protocol A, the disparity being attributable to difference in contact impedance between the two sides of the electrode associated with the reaction impedance.

The results confirm the proposed equivalent circuit for the reaction kinetic impedance (Fig. 2), *i.e.*, the contact resistance is in series with the kinetic impedance, although it does not directly result in the first semicircle in the kinetic impedance spectrum.

EIS of porous JM 287 graphite electrode.—The potential profile for the 14th lithium insertion/extraction cycle into JM 287 graphite shows typical characteristics of Li-graphite electrodes, with three potential plateaus at around 0.2, 0.1, and 0.08 V *vs.* Li due to a successive two-phase transformation. The reversible capacity was 295 mAh/g.[15] The six EIS protocols were conducted at 0.063 and 0.9 V during the 15th lithium extraction cycle (Fig. 5). Impedance spectra for JM graphite in 1 M $LiPF_6$, PC-EC-DMC (1:1:3) are similar to those for a $LaNi_{4.4}Sn_{0.25}$ electrode in 6.0 M KOH in the following respects:

1. The three kinetic impedance spectra in the lithiated state at 0.63 mV show two depressed semicircles at higher frequencies, following by a sloping line. The second semicircle (corresponding to charge transfer) was overlapped by the lithium diffusion line when Li was extracted from the graphite at 0.9 V.
2. The first depressed semicircle is present in the F protocol EIS, and the F protocol impedance is smaller than that for E. The first semicircle for D lies midway between those for F and E.
3. The protocol B impedance is almost the same to the protocol C impedance. At 0.9 V, the protocols A, B, and C impedances show two semicircles identified with particle-to-particle and particle-to-current collector contact impedances. The volume expansion on Li insertion decreases the contact impedances, which disappeared at 0.063 V.
4. The protocol E impedance is equal to the sum of protocols F and B impedances.

Therefore, as with the $LaNi_{4.4}Sn_{0.25}$ electrode, the first high frequency depressed semicircle in the kinetic impedance spectra of JM 287 graphite should also not be directly attributed to the contact impedance, although the intrinsic impedance is in series with the kinetic impedance, which contradicts recent conclusions by Chang.[12]

EIS characteristics of ion insertion porous electrodes.—The first high frequency semicircle in the kinetic impedance for graphite is usually attributed to the presence of SEI film formed during initial lithium insertion into graphite,[10,11,13,14] and to the transition between hydrogen absorption and adsorption for metal-hydride electrodes.[5-7] The oxide film covering the hydride electrode may also play an important role in defining the first semicircle of the hydride electrode.

The intrinsic impedance is in series with the kinetic impedance for both types of insertion electrode. Hence, the contact impedances should increase the kinetic impedances. The contact impedance will

affect the kinetic step, which has a similar characteristic frequency to that for the contact impedances. If the characteristic frequencies of two contact impedance semicircles are similar to that of the first high frequency kinetic impedance semicircle, and if the contact resistance is larger than SEI film resistance (for graphite), or the resistance of $H_{ad} \leftrightarrows H_{ab}$ (for hydride electrodes), the first high frequency semicircles will become more dependent on the contact resistance. This can explain why an increase in the amount of binder and a decrease in the contact area between active material and the current collector increases the size of first kinetic impedance semicircle for both graphite[12] and hydride electrodes.[4] However, if the characteristic frequency of contact impedance is low, the contact resistance may increase the resistance of charge transfer, or even the diffusion resistance for hydrogen or lithium in the host material.

Conclusions

The kinetic impedance spectra of hydrogen and lithium insertion electrodes have common characteristics, *i.e.*, two depressed semicircles in the high frequency region, following by a sloping line. The second semicircle and the line are respectively due to charge transfer and H or Li diffusion into the host material. The first high frequency depressed semicircle should not be directly attributed to the active particle-to-particle and particle-to current collector contact impedance, although about 50% of real intrinsic impedance is in series with the kinetic impedance.

Acknowledgment

We gratefully acknowledge NASA-Glenn Research Center, Cleveland, OH, for support of this work.

Texas A&M University assisted in meeting the publication costs of this article.

References

1. M. Winter, J. O. Besenhard, M. E. Spahr, and P. Novak, *Adv. Mater.*, **10**, 725 (1998).
2. Q. M. Yang, M. Ciureanu, D. H. Ryan, and J. O. Strom-Olsen, *J. Electrochem. Soc.*, **141**, 2108 (1994).
3. B. V. Ratnakumar, C. Witham, R. C. Bowman, Jr., A. Hightower, and B. Fultz, *J. Electrochem. Soc.*, **143**, 2578 (1996).
4. W. Zhang, M. P. S. Kumar, and S. Srinivasan, *J. Electrochem. Soc.*, **142**, 2935 (1995).
5. C. Wang, M. P. Soriaga, and S. Srinivasan, *J. Power Sources*, **85**, 212 (2000).
6. C. Wang, *J. Electrochem. Soc.*, **145**, 1801 (1998).
7. A. Lundqvist and G. Lindbergh, *Electrochim. Acta*, **44**, 2523 (1999).
8. N. Kuriyama, T. Sakai, H. Miyamura, I. Uehara, and H. Ishikawa, *J. Alloys Compd.*, **202**, 183 (1993).
9. N. Kuriyama, T. Sakai, H. Miyamura, I. Uehara, H. Ishikawa, and T. Iwasaki, *J. Electrochem. Soc.*, **139**, L72 (1992).
10. E. Barsoukov, J. H. Kim, J. H. Kim, C. O. Yoon, and H. Lee, *J. Electrochem. Soc.*, **145**, 2711 (1998).
11. C. R. Yang, J. Y. Song, Y. Y. Wang, and C. C. Wan, *J. Appl. Electrochem.*, **30**, 29 (2000).
12. Y. C. Chang and H. J. Sohn, *J. Electrochem. Soc.*, **147**, 50 (2000).
13. M. D. Levi and D. Aurbach, *J. Phys. Chem. B*, **101**, 4630 (1997).
14. A. Funabiki, M. Inaba, Z. Ogumi, S. Yuasa, J. Otsuji, and A. Tasaka, *J. Electrochem. Soc.*, **145**, 172 (1998).
15. C. Wang, I. Kakwan, A. J. Appleby, and F. E. Little, *J. Electroanal. Chem.*, **489**, 55 (2000).
16. C. Wang, A. J. Appleby, and F. E. Little, *J. Electroanal. Chem.*, **497**, 33 (2001).
17. C. Wang, A. J. Appleby, and F. E. Little, *Electrochim. Acta*, **46**, 1793 (2001).
18. C. Wang, A. J. Appleby, and F. E. Little, *J. Power Sources*, **93**, 174 (2001).
19. C. Wang, A. F. Rakotondrainibe, A. J. Appleby, and F. E. Little, *J. Electrochem. Soc.*, **147**, 4432 (2000).
20. G. Paasch, K. Micka, and P. Gersdorf, *Electrochim. Acta*, **38**, 2653 (1993).